nature photonics

Article

https://doi.org/10.1038/s41566-025-01668-3

Microcavity Kerr optical frequency division with integrated SiN photonics

Received: 6 March 2024

Accepted: 26 March 2025

Published online: 23 May 2025

Check for updates

Shuman Sun[1,6], Mark W. Harrington[2], Fatemehsadat Tabatabaei[1], Samin Hanifi[1], Kaikai Liu[2], Jiawei Wang[2], Beichen Wang[1], Zijiao Yang[1,3], Ruxuan Liu[1], Jesse S. Morgan[1], Steven M. Bowers[1], Paul A. Morton[4], Karl D. Nelson[5], Andreas Beling[1], Daniel J. Blumenthal[2] & Xu Yi[1,3]

Optical frequency division has revolutionized microwave and millimetre-wave generation and set spectral purity records owing to its unique capability to transfer high fractional stability from optical to electronic frequencies. Recently, rapid developments in integrated optical reference cavities and microresonator-based optical frequency combs (microcombs) have created a path to transform optical frequency division technology to the chip scale. Here we demonstrate an ultralow-phase-noise millimetre-wave oscillator by leveraging integrated photonic components and microcavity Kerr optical frequency division. The oscillator derives its stability from an integrated complementary-metal–oxide–semiconductor-compatible SiN coil cavity, and the optical frequency division is achieved spontaneously through Kerr interaction in the integrated SiN microresonator between the soliton microcombs and the injected reference lasers. Besides achieving low phase noise for integrated millimetre-wave oscillators, our demonstration greatly simplifies the implementation of integrated optical frequency division oscillators and could be useful in applications of radar, spectroscopy and astronomy.

Stable microwaves and millimetre waves (mmWaves) are of critical importance to a wide range of applications, including radar, astronomy and spectroscopy. Owing to the invention of optical frequency division (OFD)[1], the spectral purity of optically generated microwaves and mmWaves has surpassed all other approaches[1–4]. In the OFD, the high fractional stability of optical reference cavities can be coherently transferred from optical to microwave frequencies by using optical frequency combs. When phase locking the frequencies of comb lines to that of the optical reference by feedback control of the comb repetition rate, the frequency and phase of the optical reference are divided down coherently to the comb repetition rate. Stable microwaves can be produced by detecting the comb on a fast photodiode. Identical to all frequency divisions, the phase noise of the output is reduced by the square of the division ratio relative to the input signal. Recently, the rapid developments in integrated optical references[5–8] and soliton microresonator-based frequency combs (microcombs)[9–11] provide a path to miniaturize OFD to the chip scale[12–16]. The low size, weight and power of integrated OFD oscillators will extend the OFD technology to applications in the fields that demand exceedingly low microwave phase noise and portability. Furthermore, the repetition rates in soliton microcombs can reach mmWave and terahertz frequencies[12,13,17,18], which are important to applications in 5G/6G wireless communications[19], radio astronomy[20] and radar[21].

Here we report a low-phase-noise mmWave generation based on integrated photonics[13] and Kerr-induced optical frequency division (Kerr OFD)[15,22–25]. In contrast to traditional OFD, there is no servo-control

[1]Department of Electrical and Computer Engineering, University of Virginia, Charlottesville, VA, USA. [2]Department of Electrical and Computer Engineering, University of California Santa Barbara, Santa Barbara, CA, USA. [3]Department of Physics, University of Virginia, Charlottesville, VA, USA. [4]Infleqtion, Louisville, CO, USA. [5]Honeywell Aerospace Technologies, Plymouth, MN, USA. [6]Present address: T.J. Watson Laboratory of Applied Physics, California Institute of Technology, Pasadena, CA, USA. e-mail: danb@ucsb.edu; yi@virginia.edu

https://doi.org/10.1038/s41566-025-01668-3

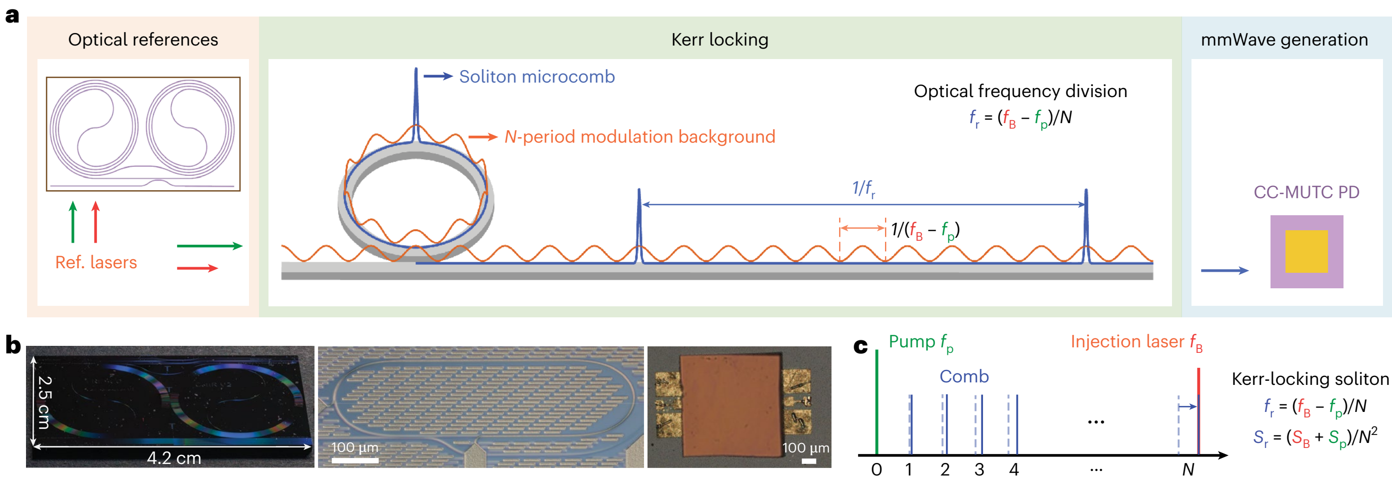

Fig. 1 | Concept of Kerr OFD for stable microwave and mmWave generation. **a**, Conceptual schematic of Kerr OFD. A pair of reference lasers (A and B) are created by stabilizing them to an integrated SiN coil reference cavity. Reference laser A is used to pump an integrated SiN microresonator to generate a soliton microcomb, and it also serves as the zeroth comb line. Reference laser B is injected into the microresonator, and its frequency is near the frequency of the *N*th comb line. Inside the microresonator, reference lasers A and B create an amplitude-modulation background, which traps solitons through the Kerr effect and synchronizes the timing of the soliton microcomb with the reference laser pair. In the time domain, the soliton repetition period is *N* times the reference laser beatnote period. In the frequency domain, the soliton repetition rate is 1/*N* of the frequency difference of the two reference lasers. As a result, the reference laser frequency difference is divided down by *N* to the soliton repetition rate. Photodetecting the soliton on a fast CC-MUTC PD generates stable microwave and mmWaves. **b**, Pictures of key photonic elements in the Kerr OFD. Left: an integrated 4-m SiN coil reference cavity. Middle: an integrated SiN microresonator with a 109.5-GHz FSR. Right: a typical flip-chip-bonded CC-MUTC PD. **c**, Frequency-domain illustration of Kerr OFD. When the soliton is Kerr locked to the reference lasers, its *N*th comb line moves from its free-running frequency (dashed line) to the injection laser frequency through the change in comb repetition rate. *S*, phase noise.

loop in the Kerr OFD. Instead, the stable optical reference lasers are circulating in the soliton microcomb resonator to directly synchronize the timing of the soliton through the Kerr effect. Although Kerr OFD has been proposed[22,25] and recently demonstrated experimentally[15,23,24] in the form of sideband injection locking or Kerr synchronization, its combination with ultrastable optical references has not been shown yet. In our oscillator, the phase stability is provided by a pair of stabilized lasers at 1,551 nm and 1,600 nm that are locked to a common complementary-metal–oxide–semiconductor-compatible integrated SiN coil reference cavity[8,13]. The reference laser at 1,551 nm (f_A) is amplified to pump the microresonator to generate soliton microcombs, and it serves as the zeroth comb line. The other reference laser at 1,600 nm (f_B) is injected into the microresonator, and its frequency is tuned to near the *N*th comb line. The two reference lasers create periodic intensity modulation inside the microresonator, which transforms into periodic refractive-index modulation through the Kerr effect and traps solitons[26,27]. This synchronizes the soliton timing with the reference lasers in the time domain, whereas in the frequency domain, the frequency difference of the two reference lasers is divided by *N* times to the soliton repetition rate f_r. The soliton is then detected on a high-speed flip-chip-bonded charge-compensated modified unitraveling carrier photodiode (CC-MUTC PD)[18,28] to generate 109.5-GHz mmWaves with exceedingly low phase noise. At 100-Hz and 10-kHz offset frequencies, the phase noise reaches −77 dBc Hz^{-1} and −121 dBc Hz^{-1}, respectively, which correspond to −98 dBc Hz^{-1} and −142 dBc Hz^{-1} when the carrier frequency is scaled to 10 GHz. To the best of our knowledge, this is the lowest phase noise for an integrated photonic mmWave oscillator (Fig. 1).

It is important to compare this Kerr OFD approach with the conventional servo-controlled OFD approach. In conventional servo OFDs, the phase error between the comb line and the optical reference is detected and is corrected by feedback control of a current or voltage that tunes the comb repetition rate. Auxiliary optoelectronic components, such as photodiodes, optical amplifiers, low-frequency local oscillator and electronic proportional–integral–derivative controls, are often necessary for conventional OFD[1,12–14]. In addition, OFD requires a large servo bandwidth, and thus, the bandwidth of all auxiliary components and the tuning mechanism of the comb repetition rate have to be high. So far, the servo bandwidths of microcomb-based OFD are limited to hundreds of kilohertz[12–14,29,30]. By contrast, the Kerr OFD leverages the strong Kerr interaction between the reference lasers and temporal solitons in the optical microresonator, and the soliton is passively locked to the optical references. No auxiliary component is needed, which greatly simplifies the implementation of OFD. In addition, a large locking bandwidth is feasible with small injection power due to the cavity-enhanced Kerr interaction. In our demonstration, the maximum locking bandwidth is estimated to reach above 30 MHz when only 185 µW of the reference laser power is injected into the cavity. We believe the demonstration of Kerr OFD paves the path for high-performance, fully integrated low-noise photonic microwave and mmWave oscillators (Fig. 2).

Results

The soliton microcomb is generated in an integrated Si_3N_4 racetrack-shape microresonator, with a cross-section of 2.5 µm (width) × 0.8 µm (height). The resonator has a free spectral range (FSR) of 109.5 GHz and an intrinsic (loaded) quality factor of 5.5 × 10^6 (3.7 × 10^6) at 1,551 nm. A fast modulation sideband of laser A (1,551 nm) serves as the pump of the soliton microcomb[31]. The pump frequency can be rapidly tuned by tuning the voltage-controlled oscillator that drives the modulator. Laser B at 1,600 nm is combined with the pump laser on a wavelength-division multiplexer and is injected into the microresonator. The optical spectra of the soliton and injection laser B are shown in Fig. 3a. Lasers A and B are external-cavity diode lasers (NewFocus Velocity TLB-6700).

The frequency of injection laser B can be tuned continuously around 1,600 nm to investigate the Kerr OFD mechanism (Fig. 3b). Figure 3c shows the photodetector signal of the transmitted injection laser B and the soliton microcomb versus the frequency of laser B. Around −1.86-GHz offset frequency, the frequency difference between laser B and comb line $N = -54$ is within the photodiode bandwidth, and the beatnote between laser B and comb line can be observed. When the *N*th comb line is locked to the injection laser, the beatnote oscillator disappears and is reduced to a d.c. voltage[23,24] (area marked by orange).

https://doi.org/10.1038/s41566-025-01668-3

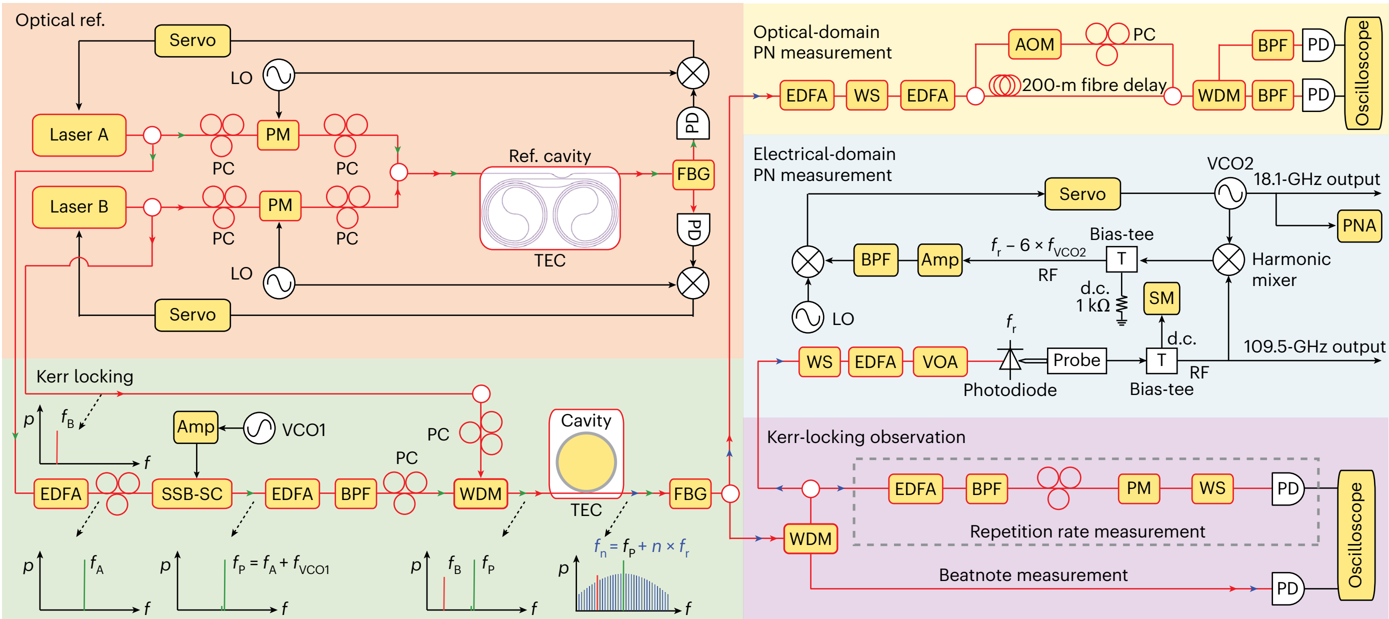

Fig. 2 | Experimental setup. Laser A and laser B are stabilized to the coil reference cavity and serve as the reference lasers. Laser A is used to create the pump laser that generates solitons in an integrated microresonator. Laser B is combined with the pump laser on a wavelength-division multiplexer (WDM) and injected into the same microresonator for Kerr locking and Kerr OFD. Both coil reference cavity and soliton microresonator are temperature controlled by thermoelectric coolers (TECs). The soliton microcomb is then split for optical-domain phase noise (PN) measurement (i), mmWave generation and electrical-domain phase noise measurement (ii) and Kerr-locking phenomenon observation (iii). Erbium-doped fibre amplifiers (EDFAs), polarization controllers (PCs), phase modulators (PMs), single-sideband suppressed carrier modulator (SSB-SC), bandpass filters (BPFs), fibre Bragg grating (FBG) filters, line-by-line waveshaper (WS), acousto-optic modulator (AOM), phase noise analyser (PNA), electrical amplifiers (Amps), source meter (SM) and variable optical attenuator (VOA) are used in the experiment.

The instantaneous frequency of the beatnote in the locking area is measured and shown in Fig. 3d. Between the frequency offset from −44 MHz to −109 MHz (Fig. 3d), no beatnote frequency can be found, which indicates that comb line $N = -54$ is locked to the injection laser within this frequency range. Out of this range, the beatnote frequency and its harmonics can be seen. The cavity resonance mode can also be observed during transmission (Fig. 3c), which is near the −0.57-GHz offset frequency. This shows that strong Kerr locking can happen when the injection laser frequency is far from the cavity resonance frequency.

Kerr locking leads to an OFD, as $f_N = f_p + N \times f_r = f_B$ and $f_r = (f_B - f_p)/N$, where f_B is the injection laser frequency (laser B), f_p is the pump frequency, f_N is Nth comb line frequency, N is the comb line number with respect to the pump and f_r is the repetition rate. The Kerr OFD can be observed by measuring the repetition rate versus the injection laser frequency[23,24] (Fig. 3e). When the injection laser frequency is in the range from −44 MHz to −109 MHz, the soliton repetition rate changes linearly with the injection laser frequency. A line with a slope of −1/54 is plotted to show the division ratio. The Kerr OFD is measured under a series of injected optical power of laser B, and the single-sided locking range versus injected power is plotted in Fig. 3f. The Kerr-locking range can also be calculated analytically[23,24] (Methods), and we have

$$|\omega_B - \omega_{s,N}| \leq 2D_2N^2 \frac{\kappa_e}{\kappa} \frac{\sqrt{P_{s,N}P_B}}{P_s} \stackrel{\text{def}}{=} \delta_{\max}, \tag{1}$$

where ω_B is the injection laser frequency, $\omega_{s,N}$ is the frequency of the Nth soliton comb line, D_2 is the microresonator dispersion, κ is the resonator dissipative rate and κ_e is the coupling rate between the microresonator and the waveguide. P_B is the on-chip injection laser power and P_s and $P_{s,N}$ are the soliton microcomb power and its Nth comb line power in the output waveguide, respectively. The measurement results show that the locking range increases with the square root of the injection laser power, which agrees with equation (1). Furthermore, the locking bandwidth of Kerr OFD can be calculated analytically under the small-signal approximation:

$$\delta_{BW} = \delta_{\max} |\cos \bar{\Theta}|, \tag{2}$$

where $\sin \bar{\Theta} = (\omega_B - \omega_{N,s})/\delta_{\max}$. The maximum locking bandwidth equals to the one-sided locking range. The locking bandwidth is important to the phase noise performance of Kerr OFD. The calculation also shows that the Kerr OFD has a 20 dB per decade gain (equation (10)), which is the same as the type-I locking loop.

The Kerr OFD can be used to generate stable microwaves and mmWaves when the pump laser and injection laser are stabilized to the integrated optical coil references. Here the reference cavity is an integrated thin-film SiN cavity with a cross-section of 6 μm (width) × 80 nm (height). The cavity is 4 m long and coiled on a chip of centimetre-scale chip[8] with the measured intrinsic (loaded) quality factors of 66×10^6 (46×10^6) and 81×10^6 (47×10^6) at 1,551 nm and 1,600 nm, respectively. The large mode volume and high quality factor together provide outstanding phase stability[8]. Both pump laser and injection laser are stabilized to the same reference cavity by using the Pound–Drever–Hall locking technique. The reference cavity is packaged to isolate technical noise from the environment. Compared with our previous work[13], the reference cavity used here exhibits a higher quality factor and is packaged to shield environmental noise. These improvements reduce the reference lasers' phase noise to the reference cavity's thermorefractive noise limit (Extended Data Fig. 1). It is worth pointing out that the FSR of our coil reference cavity is 50 MHz, which is smaller than the two-sided Kerr OFD locking bandwidth (65 MHz). As a result, there is always an optical mode of the reference cavity within the locking range to stabilize the injection laser.

To generate stable mmWaves at 109.5 GHz, the Kerr OFD solitons are then optically amplified and illuminated on a high-speed CC-MUTC

https://doi.org/10.1038/s41566-025-01668-3

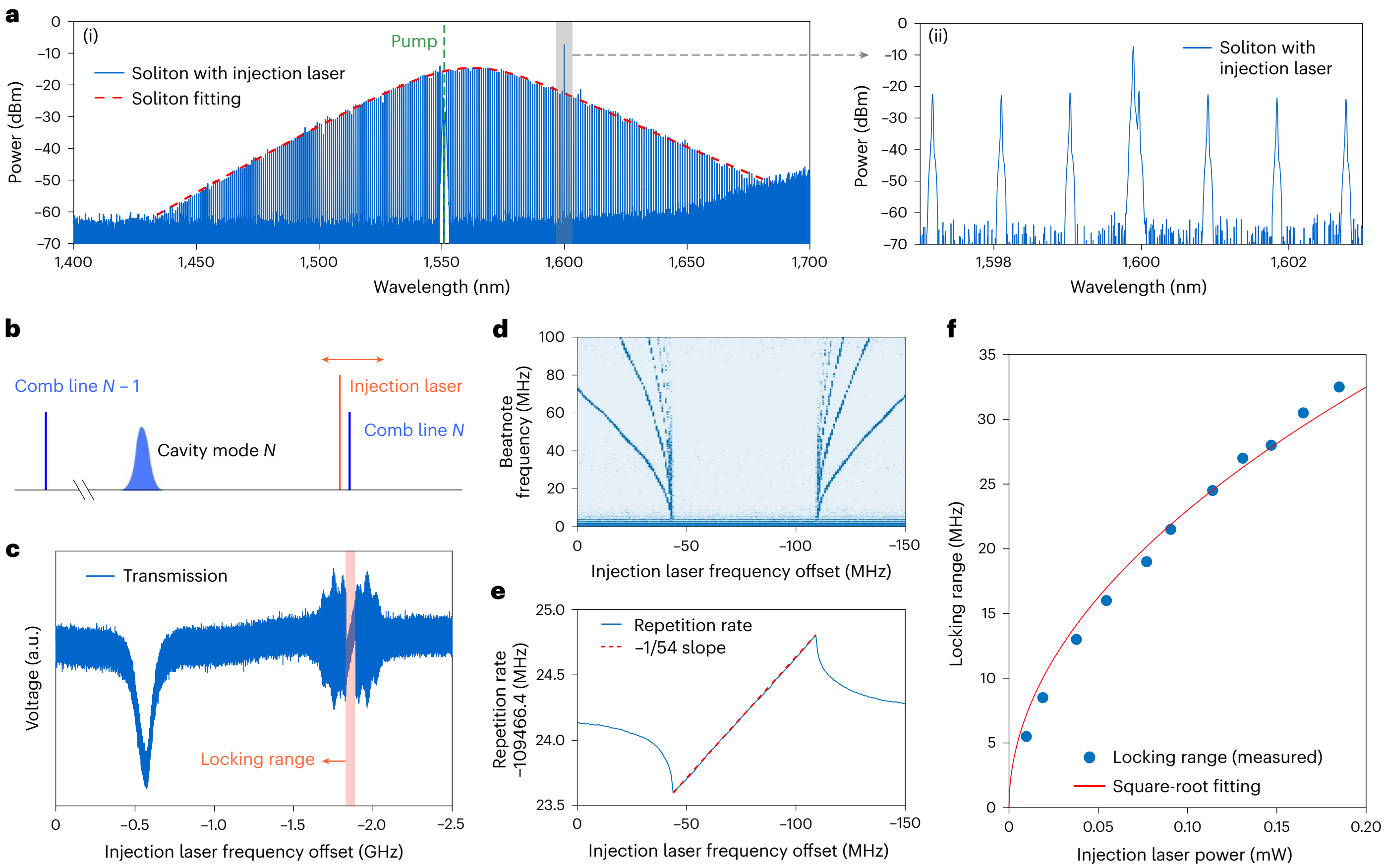

Fig. 3 | Observation of Kerr locking and Kerr OFD. a, Optical spectrum of soliton microcombs and the injection laser. A zoomed-in view of the spectrum around the injection laser wavelength is shown on the right. **b**, Illustration of the measurement in the frequency domain. The frequency of the injection laser (f_B) is scanned continuously near the *N*th comb line and *N*th cavity mode. **c**, Transmission of the injection laser and the soliton microcomb versus the frequency of the injection laser. When the frequency of the injection laser enters the Kerr-locking range (area marked by orange), comb line *N* is locked to the injection laser and the beatnote oscillator disappears and is reduced to a d.c. voltage. **d**, Spectrogram of the locking regime, which gives the instantaneous frequency of the transmission. The beatnote frequency disappears in the middle, showing that the frequency of comb line *N* is locked to the injection laser. **e**, Measured soliton repetition rate versus the injection laser frequency. A red dashed line with a slope of −1/54 is plotted in the locking region, validating the OFD. **f**, One-sided locking range is measured versus the injection laser power. The measurements are in good agreement with the squared-root fitting data (red line).

PD[18,28]. Since the carrier frequency is well above the frequency range of our phase noise analyser, a mmWave-to-microwave frequency division (mmFD) method is applied to further divide the generated 109.5-GHz mmWave down to 18.1 GHz. Details of the mmFD method have been described elsewhere[13]. After the mmFD, the spectra and phase noise of the 18.1-GHz signal can be directly measured on the phase noise analyser. The electrical spectra from both free-running soliton (orange trace) and Kerr OFD soliton (blue trace) are shown in Fig. 4b (top-right inset). The phase noise of the 18.1-GHz signal is also shown (Fig. 4b, green). Scaling the carrier frequency up to 109.5 GHz provides an upper-bound limit for the phase noise of the 109.5-GHz mmWave, and both free-running soliton (orange) and Kerr OFD soliton (blue) results are shown in Fig. 4b. For a general comparison with other oscillators, the Kerr OFD result is also scaled down to a typical 10-GHz carrier frequency and plotted as the dashed grey line. It should be noted that since the mmFD has a servo bandwidth of 312 kHz, phase noise measurement at high offset frequencies is limited by the mmFD method itself instead of the Kerr OFD. To evaluate the soliton phase noise at higher offset frequencies, a dual-tone delayed self-heterodyne interferometry method[32] is used separately, and the combined phase noise is shown in Fig. 5 (blue).

The phase noise of the generated microwave and mmWave is exceptionally low. When the carrier frequency is scaled down to 10 GHz, the phase noise reaches −142 dBc Hz^{-1} at a 10-kHz offset, which is lower than most integrated photonic microwave and mmWave oscillators. Two notable exceptions are the recent work in refs. 29,30, where the soliton microcombs are stabilized to non-integrated optical references to reach better phase noise performances. Our reported value is approximately 27 dB better than the Keysight PSG standard model commercial signal generator. At a 100-Hz offset frequency, the phase noise reaches an impressive −98 dBc Hz^{-1}. The demonstrated phase noise has notable improvement over our previous demonstration with conventional OFD[13] (Fig. 5, pink). The improvement mainly comes from two factors: (1) the improved reference cavity, which has a better quality factor and is packaged to shield environmental noises; (2) the larger OFD locking bandwidth owing to the implementation of Kerr OFD. The measurements of the reference laser comparison and the conventional OFD versus Kerr OFD comparison are shown in Extended Data Fig. 1.

In Fig. 5, we compare our results with several state-of-the-art photonic oscillators that are based on integrated soliton microcombs. All the carrier frequencies are scaled to 10 GHz for phase noise comparison. Because of the high stability and low thermorefractive noise limit of the reference cavity and the power of OFD, our oscillator outperforms the best integrated free-running soliton microwave oscillator[33] (red) and OFD-based oscillators that are referenced to integrated optical parametric oscillators (OPOs)[15] (orange) and 75-m-long optical fibre[12] (green). Compared with the best integrable photonic microwave oscillator reported so far, which is stabilized to a microfabricated

https://doi.org/10.1038/s41566-025-01668-3

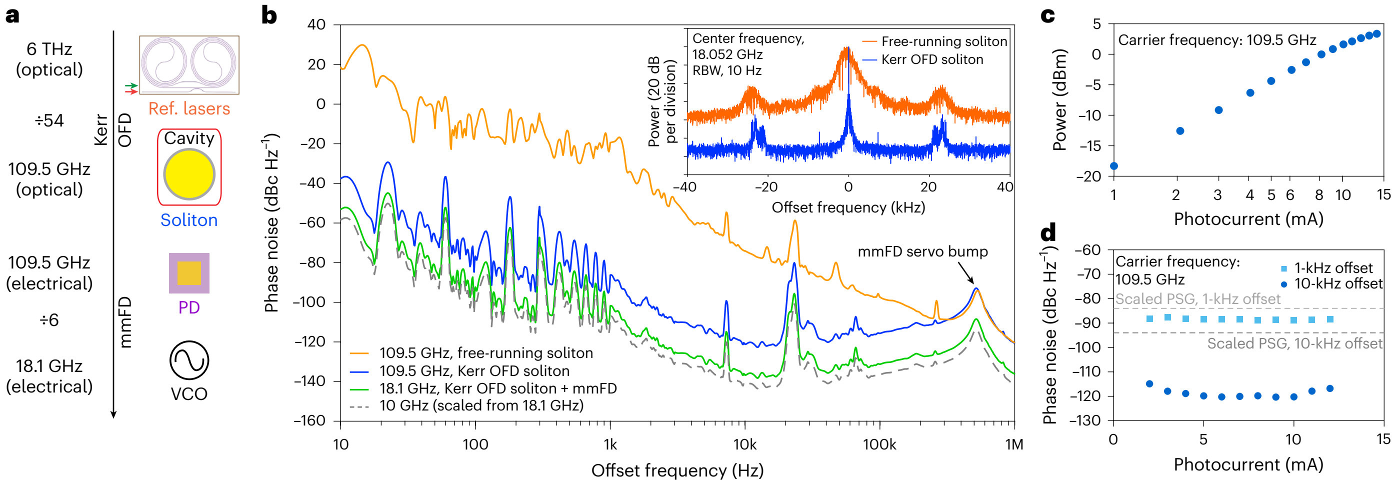

Fig. 4 | Characterization of mmWave generated from Kerr OFD. a, Illustration of phase noise measurement for the mmWave generated with Kerr OFD. The 6-THz frequency difference of the two optical reference lasers is divided down to 109.5 GHz through Kerr OFD, and the mmWave is generated on a CC-MUTC PD. To measure the phase noise of the mmWave, an mmFD is used to divide the 109.5-GHz output by 6 to the 18.1-GHz output of a voltage-controlled oscillator (VCO), whose phase noise can be directly measured using a phase noise analyser. **b**, Phase noise characterization. The phase noise of the mmWave output after mmFD at an 18.1-GHz carrier frequency is shown in green. Scaling the carrier frequency back to 109.5-GHz mmWave gives the upper bound of the mmWave phase noise (blue for the Kerr OFD soliton and orange for the free-running soliton). For a general comparison, the phase noise is also scaled to a typical 10 GHz (grey dashed line). Inset: electrical spectra of the Kerr OFD output after mmFD for the free-running soliton (orange) and Kerr OFD soliton (blue). RBW, resolution bandwidth. **c**, mmWave power versus photocurrents. The maximum output power is 3.4 dBm with photocurrents of 14 mA. **d**, Phase noise of the mmWave at 1-kHz and 10-kHz offset frequencies versus the photocurrents. For comparison, the phase noise of the Keysight PSG standard model with its carrier frequency scaled to 109.5 GHz is shown as the grey dashed lines.

Fabry–Pérot (FP) cavity[14] (purple), our oscillator performs equally well from 5-kHz to 100-kHz offset frequencies. Above the 100-kHz offset frequency, our oscillator shows lower phase noise because of the large locking bandwidth of the Kerr OFD. In comparison, there is a servo bump at a 300-kHz offset frequency for the FP-referenced oscillator. Below 5 kHz, our phase noise is higher, and we suspect that this is because our soliton microcomb setup and the MUTC PD setup are in two different rooms due to laboratory space limitation, and around 60-m-long fibre is used to connect them. This could add technical noise to the low offset frequency. The noise peak around a 25-kHz offset frequency comes from the lasers used in the system. Although the carrier frequencies of oscillators are scaled to 10 GHz for phase noise comparison, microcomb OFD oscillators at different frequency bands face very different challenges. At 100 GHz and above, the mmWave generation and phase noise characterization are more difficult than microwave frequencies. However, it is challenging for microcomb OFD oscillators to directly reach a low carrier frequency, for example, 10 GHz, and maintain a large effective division ratio, as the microcomb span typically reduces with the increase in microresonator size[33].

Finally, the mmWave power is characterized and shown in Fig. 4d. The maximum power of 3.4 dBm is obtained at a photocurrent of 14 mA. The mmWave phase noise at different photocurrents is also recorded. Results for 1-kHz offset (light-blue squares) and 10-kHz offset (dark-blue dots) are plotted in Fig. 4e, and the phase noise remains stable at different power levels. For comparison, the phase noise of the Keysight PSG signal generator (standard model) is shown in the same figure using dashed lines, and the carrier frequency has been scaled up to 109.5 GHz.

In summary, we have demonstrated low-phase-noise mmWave generation with integrated photonics using integrated coil reference-cavity-stabilized lasers and the Kerr OFD approach. Compared with conventional servo OFD, Kerr OFD is much simpler to implement and has a much larger locking bandwidth of tens of megahertz. In this work, the phase noise of the generated mmWave at a high offset frequency is limited by the reference laser, since the Pound–Drever–Hall locking loop in the reference laser has a bandwidth of only 145 kHz.

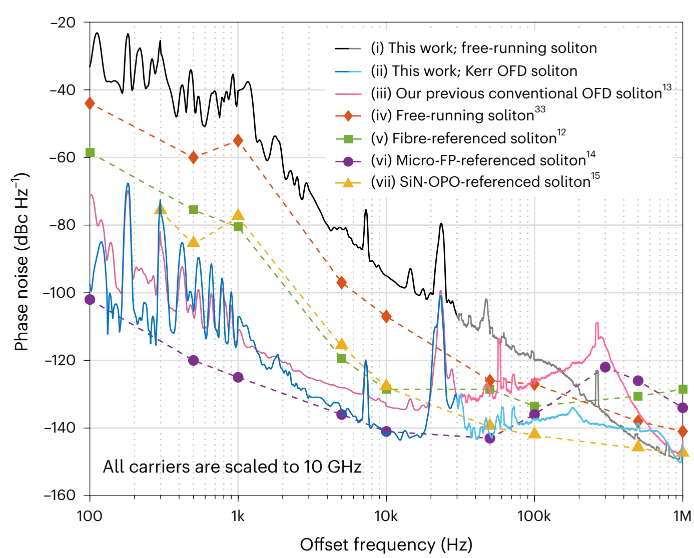

Fig. 5 | Approximate phase noise of several integrated microcomb-based microwave and mmWave oscillators. For comparison, the carrier frequency is scaled to 10 GHz for all traces. Free-running soliton phase noise of this work (i). Phase noise of the Kerr OFD soliton in this work. Original carrier frequency, 109.5 GHz (ii). Phase noise of a conventional OFD soliton in our previous work (iii)[13]. Best free-running integrated soliton microcomb (iv)[33]. Original carrier frequencies, 10 GHz and 20 GHz. SiN soliton microcomb referenced to a 75-m-long optical fibre[12]. Original carrier frequency, 300 GHz (v). Trace: integrated OFD oscillator referenced to the microfabricated FP cavity[14]. Original carrier frequency, 20 GHz (vi). Soliton microcomb referenced to an integrated OPO via all OFD[15]. Original carrier frequency, 16 GHz (vii).

This performance can be dramatically improved in the future by using an optical reference based on a stimulated Brillouin laser[34–37] or a self-injection-locked laser[7]. Increasing the division ratio N can further improve the phase noise performance, and this can be achieved by moving the injection laser frequency further away from the soliton centre. Although the lower comb line power at larger N may decrease the Kerr OFD locking bandwidth[23], this can be overcome by introducing dispersive waves to boost the comb line power by several orders of magnitude[10,30,38]. Finally, only 185 μW of the injection laser power is used in our low-phase-noise Kerr OFD oscillator and no amplification of the injection laser is necessary. This shows that the optical amplifier can be eliminated in low-noise integrated OFD oscillators in the future when the Kerr OFD is combined with soliton microcombs that are directly pumped by laser diodes[39,40].

Online content

Any methods, additional references, Nature Portfolio reporting summaries, source data, extended data, supplementary information, acknowledgements, peer review information; details of author contributions and competing interests; and statements of data and code availability are available at https://doi.org/10.1038/s41566-025-01668-3.

References

1. Fortier, T. M. et al. Generation of ultrastable microwaves via optical frequency division. *Nat. Photon.* **5**, 425–429 (2011).
2. Xie, X. et al. Photonic microwave signals with zeptosecond-level absolute timing noise. *Nat. Photon.* **11**, 44–47 (2017).
3. Nakamura, T. et al. Coherent optical clock down-conversion for microwave frequencies with 10^{-18} instability. *Science* **368**, 889–892 (2020).
4. Li, J. & Vahala, K. Small-sized, ultra-low phase noise photonic microwave oscillators at X-Ka bands. *Optica* **10**, 33–34 (2023).
5. Lee, H. et al. Spiral resonators for on-chip laser frequency stabilization. *Nat. Commun.* **4**, 2468 (2013).
6. Jin, W. et al. Hertz-linewidth semiconductor lasers using CMOS-ready ultra-high-*Q* microresonators. *Nat. Photon.* **15**, 346–353 (2021).
7. Li, B. et al. Reaching fiber-laser coherence in integrated photonics. *Opt. Lett.* **46**, 5201–5204 (2021).
8. Liu, K. et al. 36 Hz integral linewidth laser based on a photonic integrated 4.0 m coil resonator. *Optica* **9**, 770–775 (2022).
9. Herr, T. et al. Temporal solitons in optical microresonators. *Nat. Photon.* **8**, 145–152 (2014).
10. Brasch, V. et al. Photonic chip–based optical frequency comb using soliton Cherenkov radiation. *Science* **351**, 357–360 (2016).
11. Kippenberg, T. J., Gaeta, A. L., Lipson, M. & Gorodetsky, M. L. Dissipative Kerr solitons in optical microresonators. *Science* **361**, eaan8083 (2018).
12. Tetsumoto, T. et al. Optically referenced 300 GHz millimetre-wave oscillator. *Nat. Photon.* **15**, 516–522 (2021).
13. Sun, S. et al. Integrated optical frequency division for microwave and mmWave generation. *Nature* **627**, 540–545 (2024).
14. Kudelin, I. et al. Photonic chip-based low-noise microwave oscillator. *Nature* **627**, 534–539 (2024).
15. Zhao, Y. et al. All-optical frequency division on-chip using a single laser. *Nature* **627**, 546–552 (2024).
16. He, Y. et al. Chip-scale high-performance photonic microwave oscillator. *Sci. Adv.* **10**, eado9570 (2024).
17. Zhang, S. et al. Terahertz wave generation using a soliton microcomb. *Opt. Express* **27**, 35257–35266 (2019).
18. Wang, B. et al. Towards high-power, high-coherence, integrated photonic mmwave platform with microcavity solitons. *Light: Sci. Appl.* **10**, 4 (2021).
19. Rappaport, T. S. et al. Wireless communications and applications above 100 GHz: opportunities and challenges for 6G and beyond. *IEEE Access* **7**, 78729–78757 (2019).
20. Clivati, C. et al. A VLBI experiment using a remote atomic clock via a coherent fibre link. *Sci. Rep.* **7**, 40992 (2017).
21. Ghelfi, P. et al. A fully photonics-based coherent radar system. *Nature* **507**, 341–345 (2014).
22. Taheri, H., Matsko, A. B. & Maleki, L. Optical lattice trap for Kerr solitons. *Eur. Phys. J. D* **71**, 153 (2017).
23. Wildi, T., Ulanov, A., Englebert, N., Voumard, T. & Herr, T. Sideband injection locking in microresonator frequency combs. *APL Photon.* **8**, 120801 (2023).
24. Moille, G. et al. Kerr-induced synchronization of a cavity soliton to an optical reference. *Nature* **624**, 267–274 (2023).
25. Matsko, A. B. & Maleki, L. Low threshold Kerr solitons. *Opt. Lett.* **48**, 715–718 (2023).
26. Jang, J. K., Erkintalo, M., Coen, S. & Murdoch, S. G. Temporal tweezing of light through the trapping and manipulation of temporal cavity solitons. *Nat. Commun.* **6**, 7370 (2015).
27. Lu, Z. et al. Synthesized soliton crystals. *Nat. Commun.* **12**, 3179 (2021).
28. Xie, X. et al. Improved power conversion efficiency in high-performance photodiodes by flip-chip bonding on diamond. *Optica* **1**, 429–435 (2014).
29. Jin, X. et al. Microresonator-referenced soliton microcombs with zeptosecond-level timing noise. *Nat. Photon.* https://doi.org/10.1038/s41566-025-01669-2 (2025).
30. Ji, Q.-X. et al. Dispersive-wave-agile optical frequency division. *Nat. Photon.* https://doi.org/10.1038/s41566-025-01667-4 (2025).
31. Stone, J. R. et al. Thermal and nonlinear dissipative-soliton dynamics in Kerr-microresonator frequency combs. *Phys. Rev. Lett.* **121**, 063902 (2018).
32. Kwon, D. et al. Reference-free, high-resolution measurement method of timing jitter spectra of optical frequency combs. *Sci. Rep.* **7**, 40917 (2017).
33. Liu, J. et al. Photonic microwave generation in the X- and K-band using integrated soliton microcombs. *Nat. Photon.* **14**, 486–491 (2020).
34. Lee, H. et al. Chemically etched ultrahigh-*Q* wedge-resonator on a silicon chip. *Nat. Photon.* **6**, 369–373 (2012).
35. Gundavarapu, S. et al. Sub-hertz fundamental linewidth photonic integrated Brillouin laser. *Nat. Photon.* **13**, 60–67 (2019).
36. Liu, K. et al. Integrated photonic molecule Brillouin laser with a high-power sub-100-MHz fundamental linewidth. *Opt. Lett.* **49**, 45–48 (2024).
37. Heffernan, B. M., Greenberg, J., Hori, T., Tanigawa, T. & Rolland, A. Brillouin laser-driven terahertz oscillator up to 3 THz with femtosecond-level timing jitter. *Nat. Photon.* **18**, 1263–1268 (2024).
38. Yang, Q.-F., Yi, X., Yang, K. Y. & Vahala, K. Spatial-mode-interaction-induced dispersive-waves and their active tuning in microresonators. *Optica* **3**, 1132–1135 (2016).
39. Stern, B., Ji, X., Okawachi, Y., Gaeta, A. L. & Lipson, M. Battery-operated integrated frequency comb generator. *Nature* **562**, 401–405 (2018).
40. Xiang, C. et al. Laser soliton microcombs heterogeneously integrated on silicon. *Science* **373**, 99–103 (2021).

Methods

Theoretical calculations of Kerr OFD

The Kerr OFD system consists of soliton microcombs and an additional laser injected into the soliton-forming Kerr micoresonator. This can be described by the modified Lugiato–Lefever equation (LLE)[23,41], and the locking range has been solved analytically using the momentum method[22,25,41] or the Lagrangian perturbation method[23].

The equation of motion of the soliton field can be expressed as

$$\begin{aligned}\frac{\mathrm{d}A(\phi,t)}{\mathrm{d}t} = \mathrm{i}\frac{D_2}{2}\frac{\partial^2 A}{\partial\phi^2} + \mathrm{i}g|A|^2A - \mathrm{i}\delta\omega A - \frac{\kappa}{2}A + \sqrt{\kappa_\mathrm{e}P_\mathrm{p}} \\ + \mathrm{i}g\tau_\mathrm{R}D_1A\frac{\partial|A|^2}{\partial\phi} + \sqrt{\kappa_\mathrm{e}}b\mathrm{e}^{\mathrm{i}N\phi},\end{aligned} \tag{3}$$

where $A(\phi, t)$ is the optical field of the soliton in the microcavity; ϕ is the angular coordinate in the rotational frame; D_2 is the coefficient associated with group-velocity dispersion; g is the normalized Kerr nonlinear coefficient; $\delta\omega$ is the cavity–laser detuning; κ is the dissipative rate of the resonator; κ_e is the coupling rate between the resonator and the waveguide; P_p is the power of the pump laser; τ_R is the time constant of the Raman effect; D_1 is the FSR at the pumping mode; and b is the field of the laser injected into the soliton-forming microresonator, which is roughly N FSR away from the pump laser. $|A|^2$ and $|b|^2$ are normalized to the optical energy and optical power, respectively. By following the same procedure as in the counterpropagating soliton locking calculation[41], the following equation can be derived from equation (3):

$$\begin{aligned}\frac{\partial\mu_\mathrm{c}}{\partial t} &= -\kappa\mu_\mathrm{c} + \kappa\mu_\mathrm{R} + \frac{N\sqrt{\kappa_\mathrm{e}}}{E_\mathrm{s}}(a_Nb^* + a_N^*b) \\ &= -\kappa\mu_\mathrm{c} + \kappa\mu_\mathrm{R} + \frac{2N\sqrt{\kappa_\mathrm{e}}}{E_\mathrm{s}}|a_Nb|\sin\Theta,\end{aligned} \tag{4}$$

where μ_c is the mode number of the soliton spectral centre, μ_R is the soliton spectral centre shift induced by the Raman self-frequency shift effect[42] and $\mu = 0$ corresponds to the mode being pumped by the pump laser. E_s is the intracavity energy of the soliton. a_N is the intracavity field of the Nth comb line of the soliton, and $\Theta = \theta_{\mathrm{s},N} - \theta_\mathrm{B} + \pi/2$ is the phase difference between the Nth soliton comb line (a_N) and the injection optical field (b). Note that $b = \sqrt{P_\mathrm{B}}\mathrm{e}^{-\mathrm{i}\Delta\omega t}$, where $\Delta\omega = \omega_\mathrm{B} - (\omega_\mathrm{p} + D_1N)$ is the injection laser frequency in the rotation frame. Similarly, $a_N = |a_N|\mathrm{e}^{-\mathrm{i}(\omega_{N,\mathrm{s}}-\omega_\mathrm{p}-D_1N)t+\mathrm{i}\varphi}$, where $\omega_{N,\mathrm{s}}$ is the frequency of the Nth soliton comb line, φ is the overall phase of the soliton envelope and $\omega_{N,\mathrm{s}} = \omega_\mathrm{p} + N\omega_\mathrm{r} = \omega_\mathrm{p} + N(D_1 + D_2\mu_\mathrm{c})$. Therefore, $\frac{\partial\Theta}{\partial t}$ can be expressed as $\frac{\partial\Theta}{\partial t} = \Delta\omega - ND_2\mu_\mathrm{c}$. Taking the derivative of this relationship, we get

$$\begin{aligned}\frac{\partial^2\Theta}{\partial t^2} + \kappa\frac{\partial\Theta}{\partial t} &= \kappa\delta - \frac{2N^2D_2\sqrt{\kappa_\mathrm{e}}}{E_\mathrm{s}}|a_Nb|\sin\Theta \\ &= \kappa\delta - \frac{2\kappa_\mathrm{e}N^2D_2}{P_\mathrm{s}}\sqrt{P_{\mathrm{s},N}P_\mathrm{B}}\sin\Theta,\end{aligned} \tag{5}$$

where $\delta = \omega_\mathrm{B} - \omega_{N,\mathrm{s}}$ is the frequency difference between the injection laser and the Nth line of the free-running soliton. Using the input–output relationship, the intracavity field (a_N) and energy (E_s) can be converted into optical power in the output waveguide, which can be measured directly. P_s and $P_{\mathrm{s},N}$ are the optical power of the soliton microcombs and its Nth comb line in the output waveguide, respectively.

Kerr OFD locking range

The locking range of Kerr OFD can be obtained from the steady-state solution of equation (5). In the steady state, equation (5) has the solution

$$\delta = \frac{2\kappa_\mathrm{e}N^2D_2}{\kappa P_\mathrm{s}}\sqrt{P_{\mathrm{s},N}P_\mathrm{B}}\sin\Theta. \tag{6}$$

Since $|\sin\Theta| \le 1$, the steady-state solution only exists when

$$|\delta| \le 2N^2D_2\frac{\kappa_\mathrm{e}}{\kappa}\frac{\sqrt{P_{\mathrm{s},N}P_\mathrm{B}}}{P_\mathrm{s}} \overset{\mathrm{def}}{=} \delta_\mathrm{max}. \tag{7}$$

The locking range of Kerr OFD can then be found as $|\omega_\mathrm{B} - \omega_{N,\mathrm{s}}| = |\delta| \le \delta_\mathrm{max}$.

Kerr OFD bandwidth and gain

The locking bandwidth and gain are important metrics for OFD. Both of them can be analytically calculated by applying small-signal analysis to equation (5). In the small-signal approximation, we can define $\delta = \bar{\delta} + \Delta\delta$ and $\Theta = \bar{\Theta} + \Delta\theta$, where $\bar{\delta}$ and $\bar{\Theta}$ are the mean value of δ and Θ, respectively. Equation (5) then becomes

$$\frac{\partial^2\Delta\theta}{\partial t^2} + \kappa\frac{\partial\Delta\theta}{\partial t} = \kappa\Delta\delta - \kappa\delta_\mathrm{max}\Delta\theta\cos\bar{\Theta}. \tag{8}$$

From $\Theta = \theta_{\mathrm{s},N} - \theta_\mathrm{B} + \pi/2$, we can have $\Delta\theta = \Delta\varphi_\mathrm{p} + N \times \Delta\varphi_\mathrm{r} - \Delta\varphi_\mathrm{B}$, where $\Delta\varphi_\mathrm{p}$, $\Delta\varphi_\mathrm{B}$ and $\Delta\varphi_\mathrm{r}$ are the small-phase variation of the pump laser, injection laser and soliton repetition rate, respectively. Similarly, $\Delta\delta = \Delta\omega_\mathrm{B} - \Delta\omega_\mathrm{p} - N\Delta\omega_\mathrm{r}^\mathrm{free}$, where $\Delta\omega_\mathrm{p}$, $\Delta\omega_\mathrm{B}$ and $\Delta\omega_\mathrm{r}^\mathrm{free}$ are the small-frequency variation of the pump laser, injection laser and free-running soliton repetition rate, respectively. To calculate the phase noise of the soliton repetition rate in Kerr OFD, we can apply Fourier transform to equation (8) and use the general relationship between the phase and frequency ($\omega = -\partial\varphi/\partial t$) to arrive at

$$\begin{aligned}\tilde{\varphi}_\mathrm{r}(s) = \left(1 + \frac{\mathrm{i}\kappa s}{s^2 - \mathrm{i}\kappa s - \kappa\delta_\mathrm{max}\cos\bar{\Theta}}\right) \times \frac{\varphi_\mathrm{B}(s) - \varphi_\mathrm{p}(s)}{N} \\ + \frac{\mathrm{i}\kappa s}{s^2 - \mathrm{i}\kappa s - \kappa\delta_\mathrm{max}\cos\bar{\Theta}} \times \tilde{\varphi}_\mathrm{r}^\mathrm{free}(s),\end{aligned} \tag{9}$$

where $\tilde{\varphi}(s)$ is the Fourier transform of phase $\Delta\varphi$, and s is offset frequency from the carrier. As soliton repetition rate phase noise is $L_\mathrm{r}(s) = |\tilde{\varphi}_\mathrm{r}(s)|^2$, we arrive at

$$\begin{aligned}L_\mathrm{r}(s) = \left|1 + \frac{\mathrm{i}\kappa s}{s^2 - \mathrm{i}\kappa s - \kappa\delta_\mathrm{max}\cos\bar{\Theta}}\right|^2 \times \frac{L_\mathrm{B}(s) - L_\mathrm{p}(s)}{N^2} \\ + \frac{1}{1 + |\delta_\mathrm{max}\cos\bar{\Theta}/s - s/\kappa|^2} \times L_\mathrm{r}^\mathrm{free}(s).\end{aligned} \tag{10}$$

The first term on the right of the equation gives the $1/N^2$ phase noise reduction factor in OFD. The second term on the right of the equation gives the gain that suppresses the phase noise of the free-running soliton repetition rate. In the case of $s \ll \kappa$, the Kerr OFD gain reduces 20 dB per decade with the increase in offset frequency s, until the offset frequency approaches $\delta_\mathrm{max}\cos\bar{\Theta}$. In this work, $\kappa/2\pi \approx 52$ MHz. Therefore, the Kerr OFD servo bandwidth can be approximated to $\delta_\mathrm{BW} = \delta_\mathrm{max}|\cos\bar{\Theta}|$. Another observation is that the 20 dB per decade change in gain is identical to the type-I phase-locked loop.

Data availability

Data for Figs. 3–5 and Extended Data Fig. 1 are available via Figshare at https://doi.org/10.6084/m9.figshare.27629772 (ref. 43).

Code availability

The codes that support the findings of this study are available from the corresponding authors upon reasonable request.

References

41. Yang, Q.-F., Yi, X., Yang, K. & Vahala, K. Counter-propagating solitons in microresonators. *Nat. Photon.* **11**, 560–564 (2017).
42. Yi, X., Yang, Q.-F., Yang, K. Y. & Vahala, K. Theory and measurement of the soliton self-frequency shift and efficiency in optical microcavities. *Opt. Lett.* **41**, 3419–3422 (2016).

43. Sun, S. et al. Raw data for 'microcavity Kerr optical frequency division with integrated SiN photonics'. *Figshare* https://doi.org/10.6084/m9.figshare.27629772 (2025).

Acknowledgements

We acknowledge M. Woodson and S. Estrella from Freedom Photonics for the MUTC PD fabrication, Ligentec for SiN microresonator fabrication and Q.-X. Ji at the California Institute of Technology for helpful discussion. We also acknowledge DARPA GRYPHON (HR0011-22-2-0008, all authors), National Science Foundation (2023775; S.S., F.T., S.H., B.W., Z.Y., R.L., J.S.M., S.M.B., A.B. and X.Y.) and the Air Force Office of Scientific Research (FA9550-21-1-0301; S.S., B.W., Z.Y., R.L. and X.Y.). The views and conclusions contained in this document are those of the authors and should not be interpreted as representing official policies of DARPA, ARPA-E or the US Government.

Author contributions

X.Y. and S.S. designed the experiments. S.S., F.T. and S.H. performed the system measurements. M.W.H., K.L., J.W., D.J.B., K.D.N. and P.A.M. developed the reference lasers. J.S.M. and A.B. designed and fabricated the CC-MUTC PDs. S.S., X.Y., F.T. and S.H. analysed the experimental results. X.Y., D.J.B., A.B., S.M.B., P.A.M. and K.D.N. supervised and led the scientific collaboration. All authors participated in preparing the manuscript.

Competing interests

The authors declare no competing interests.

Additional information

Extended data is available for this paper at https://doi.org/10.1038/s41566-025-01668-3.

Correspondence and requests for materials should be addressed to Daniel J. Blumenthal or Xu Yi.

Peer review information *Nature Photonics* thanks David Moss and the other, anonymous, reviewer(s) for their contribution to the peer review of this work.

https://doi.org/10.1038/s41566-025-01668-3

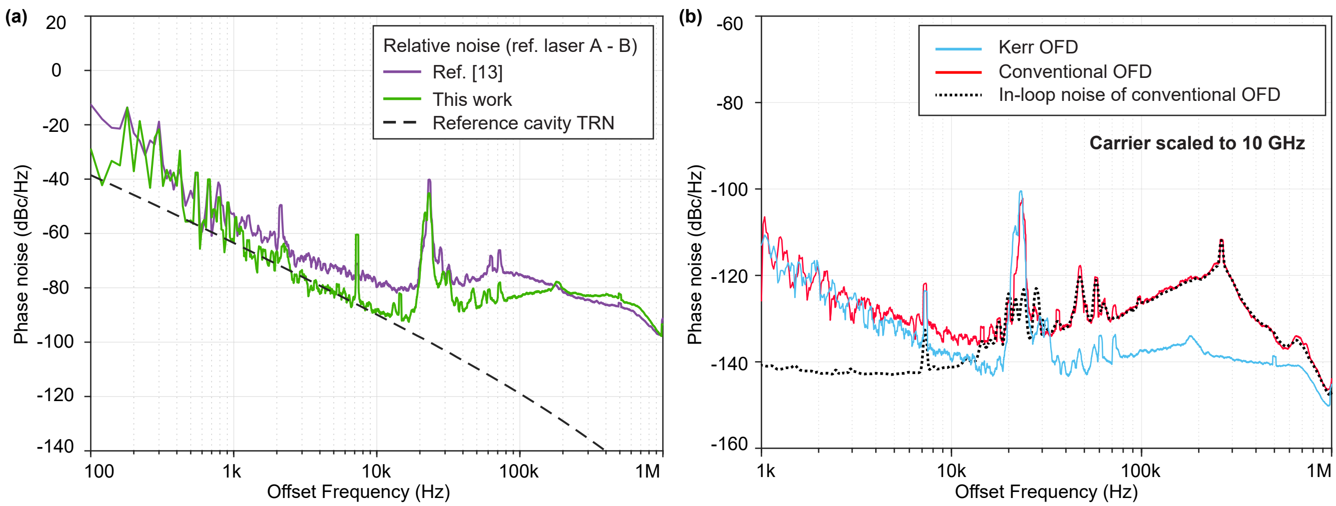

Extended Data Fig. 1 | Phase noise comparison in different OFD systems. (**a**) Phase noise comparison of reference lasers used in ref. 13 and in this work. While the length of the coil reference cavities is both 4 meters, the quality factor of the cavity in this work is improved, and the reference cavity is now packaged to isolate environmental noises. The reference laser in this work reaches the thermal refractive noise limit between 1 kHz to 10 kHz offset frequency. **(b)** Phase noise comparison of conventional OFD[13] versus the Kerr OFD in this work. The same reference lasers and soliton microcomb are used for both OFD oscillators. The conventional OFD in our setup has a servo bandwidth around 150 kHz, and the in-loop noise is limiting phase noise starting around 10 kHz offset frequency. In the low offset frequency, both methods give similar phase noise results. The phase noise in both panel (**a**) and (**b**) are measured by using optical interferometry method.